

Long-slit Spectroscopy of Edge-on Low Surface Brightness Galaxies

Wei Du^{1,2}, Hong Wu¹, Yinan Zhu¹, WeiKang Zheng³, and Alexei V. Filippenko³

¹ Key Laboratory of Optical Astronomy, National Astronomical Observatories, Chinese Academy of Sciences, 20A Datun Road, Chaoyang District, Beijing, 100012, China

² email: wdu@nao.cas.cn

³ Department of Astronomy, University of California, Berkeley, CA 94720-3411, USA

Received _____; accepted _____

ABSTRACT

We present long-slit optical spectra of 12 edge-on low surface brightness galaxies (LSBGs) positioned along their major axes. After performing reddening corrections for the emission-line fluxes measured from the extracted integrated spectra, we measured the gas-phase metallicities of our LSBG sample using both the $[\text{N II}]/\text{H}\alpha$ and the R_{23} diagnostics. Both sets of oxygen abundances show good agreement with each other, giving a median value of $12 + \log(\text{O}/\text{H}) = 8.26$ dex. In the luminosity-metallicity plot, our LSBG sample is consistent with the behavior of normal galaxies. In the mass-metallicity diagram, our LSBG sample has lower metallicities for lower stellar mass, similar to normal galaxies. The stellar masses estimated from z -band luminosities are comparable to those of prominent spirals. In a plot of the gas mass fraction versus metallicity, our LSBG sample generally agrees with other samples in the high gas mass fraction space. Additionally, we have studied stellar populations of 3 LSBGs which have relatively reliable spectral continua and high signal-to-noise ratios, and qualitatively conclude that they have a potential dearth of stars with ages < 1 Gyr instead of being dominated by stellar populations with ages > 1 Gyr. Regarding the chemical evolution of our sample, the LSBG data appear to allow for up to 30% metal loss, but we cannot completely rule out the closed-box model. Additionally, we find evidence that our galaxies retain up to about 3 times as much of their metals compared with dwarfs, consistent with metal retention being related to galaxy mass. In conclusion, our data support the view that LSBGs are probably just normal disk galaxies continuously extending to the low end of surface brightness.

Subject headings: methods: observational — techniques: spectroscopy — galaxies: abundances — galaxies: evolution — galaxies: star formation — galaxies: stellar

content

1. Introduction

Low surface brightness galaxies (LSBGs) were theorized to exist by Disney (1976) and then verified by the discovery of Malin 1 (Bothun et al. 1987). They refer to galaxies which have lower surface brightness than the background (Impey & Bothun 1997) and are traditionally defined as galaxies with central surface brightness $\mu_B(0)$ fainter than some threshold which varies between 22.0 and 23.0 mag arcsec⁻² (e.g., Impey et al. 2001; Ceccarelli et al. 2012). Recent studies indicate that LSBGs contribute 20% of the dynamical mass of galaxies in the Universe (Minchin et al. 2004) and 30%–60% of the number density of local galaxies (McGaugh 1996; Bothun et al. 1997; O’Neil et al. 2000; Trachternach et al. 2006; Habertzettl et al. 2007), suggesting that the contribution of LSBGs to the Universe can not be negligible. However, selection effects cause LSBGs to be underrepresented in the present-day galaxy catalogs.

Compared with disk galaxies having high surface brightness (HSB), LSBGs generally tend to be dust-poor (e.g., Matthews & Wood 2001) and H I-rich, with diffuse, low-density stellar disks and metallicity $\leq 1/3$ solar abundance (e.g., McGaugh 1994). This suggests that LSBGs have been inefficient star formers over their lifetimes and have low-level star-formation activity at present (e.g., Das et al. 2009; Galaz et al. 2011). Indeed, H I surface densities in LSBGs are often observed to be well below the critical threshold for star formation (e.g., van der Hulst et al. 1993). Nonetheless, LSBGs typically contain some signatures of ongoing star formation, including modest amounts of H α emission from a very small number of H II regions Schombert et al. (e.g., 1992, 2013) and blue colors indicative of young stellar populations (e.g., McGaugh & Bothun 1994; Matthews & Gallagher 1997).

Metallicities of stars and gas within a galaxy provide both a fossil record of its star formation history (SFH) and evolution. For galaxies, metallicities are traditionally represented by the oxygen abundance, $12 + \log(\text{O}/\text{H})$, which directly reflects the metal

content of the gas in galaxies and indirectly reveals the metal content of the stars in galaxies that ionize the gas. For LSBGs, many previous works have demonstrated that LSBGs are metal-poor. The LSBG sample of McGaugh (1994) has been measured to have low oxygen abundances, $12 + \log(\text{O}/\text{H}) \leq 8.4$ dex. Burkholder et al. (2001) found a mean value $12 + \log(\text{O}/\text{H}) = 8.22$ dex for 17 LSBGs. Lam et al. (2015) studied KKR17, an LSBG dominated by H I, and measured an average $12 + \log(\text{O}/\text{H}) = 8.0$ dex. The oxygen abundances of de Naray (2004) are $12 + \log(\text{O}/\text{H}) \approx 7.8\text{--}8.2$ dex. Apparently, most LSBGs have $12 + \log(\text{O}/\text{H})$ lower than the solar value of oxygen abundance of $12 + \log(\text{O}/\text{H}) = 8.87$ dex (Grevesse et al. 1996), and even lower than the transition value ($12 + \log(\text{O}/\text{H}) = 8.4$ dex) between metal-poor and metal-rich branches for the R_{23} method (see §4.3). To derive gas-phase metallicities of LSBGs, spectra should be required. However, it is not easy to derive spectra of LSBGs due to their low surface brightness. Fortunately, we have carried out spectroscopic observations for a sample of LSBGs. Later in this paper, we will introduce this observation and then study properties which are mainly relevant to metallicities on basis of the observational data.

Given the faint nature of LSBGs, with peak surface brightness $\mu_B(0) \geq 22.5$ mag arcsec⁻², it is extremely difficult to obtain spectra of their stellar continua with relatively high signal-to-noise ratio (> 10) because the sky background always dominates the signal. Studies of the stellar populations of LSBGs are currently underrepresented and are based mainly on spectra of their H II regions (e.g., Schombert et al. 2013) and central portions (e.g., Morelli et al. 2012). But the bright H II regions contain a large fraction of O- and B-type stars, so stellar populations studied through spectra of the H II regions would be biased to younger ages. Compared to observing face-on LSBGs (Du et al. 2015, e.g.,) or fiber spectroscopy, the spectral qualities can be highly improved by observing edge-on LSBGs, especially those having thin disks, with a single slit of appropriate length and width, positioned along the major axis. This scheme makes it possible, although still

very difficult, to obtain reasonable-quality data. Very fortunately, spectra of several few LSBGs of our sample have relatively reliable stellar continua which can be used for stellar population studies, so we additionally study stellar populations of these few LSBGs and to investigate their star formation histories as byproducts of our observations (§6.1).

The outline of this paper is as follows. Section 2 describes our sample, and detailed accounts of the observations and data reduction are given in §3 and §4. We study the physical properties of our edge-on LSBGs in §5, including oxygen abundances in §5.1, the luminosity-metallicity relation in §5.2, the mass-metallicity relation in §5.3, and the behavior of gas mass fraction versus metallicity in §5.4. In Section 6, we discuss stellar populations in §6.1, stellar mass estimation in §6.2, chemical evolution in §6.3, and the true nature of our LSBG sample in §6.4. Finally, we conclude in §7.

2. The Sample

A catalog of edge-on disk galaxies in SDSS DR7 (EGIS; Bizyaev et al. 2014) consists of 5747 genuine edge-on galaxies in the Sloan Digital Sky Survey (SDSS; Abazajian et al. 2009). By analyzing photometric profiles in each of the g -, r -, and i -band images, the EGIS catalog provides estimates for structural parameters of the stellar disks of the galaxies, such as the disk scale height (h), radial scale length (z_0), and central surface brightness (μ_0). To further study the EGIS catalog in combination with H I data, we correlated it with the $\alpha.40$ catalog (Haynes et al. 2011), which lists H I line sources from 40% of the area of the final blind 21 cm H I ALFALFA (Arecibo Legacy Fast Arecibo L-band Feed Array) survey for local galaxies. Using the transformation formula of Smith et al. (2002), we derived the central surface brightness in the B band, $\mu_0(B)$, from those in the g and r bands. Then, according to a widely used definition of a LSBG, there are 287 galaxies in the EGIS- $\alpha.40$ sample that can be identified as LSBGs with $\mu_0(B) > 22.5 \text{ mag arcsec}^{-2}$.

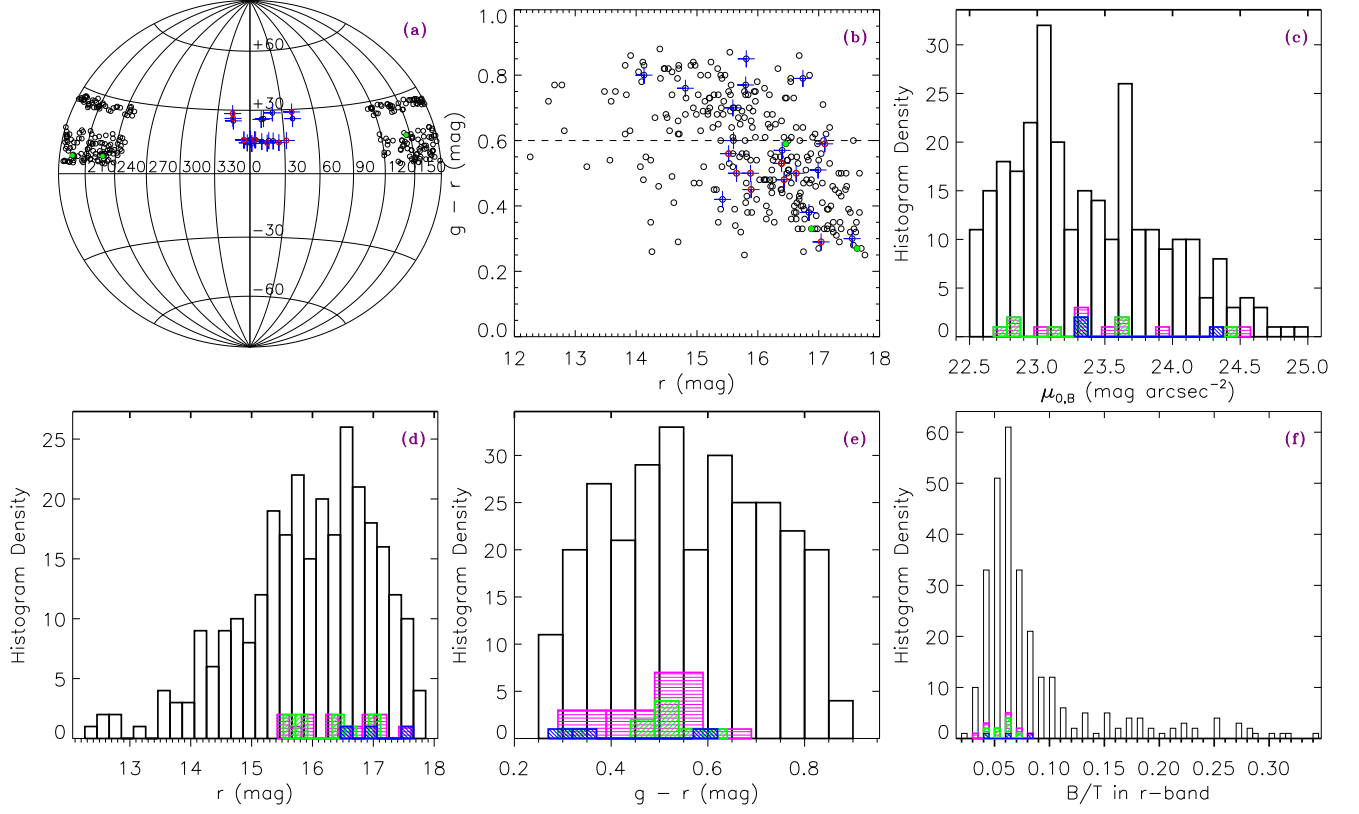


Fig. 1.— Main property distributions of 12 edge-on LSBGs in comparison with the total EGIS- $\alpha.40$ LSBG sample. In (a) and (b), blue plus signs are the 21 galaxies in the Fall sky region, black open circles show the entire EGIS- $\alpha.40$ LSBG sample, red open circles indicate the final observed 9 galaxies, and green filled circles show the 3 edge-on LSBGs observed in the Spring sky during another program. In (c)–(f), the black, magenta with line fill, green with line fill, and blue with line fill respectively represent distributions of the entire EGIS- $\alpha.40$ LSBG sample, the prepared 14 LSBG targets, the final observed 9 LSBGs, and the 3 LSBGs from another observational program. The dashed black line in (b) shows $g-r = 0.6$ mag.

Out of the EGIS- α .40 LSBG sample, only 21 galaxies (blue filled circles in Figure 1(a),(b)) are in the Fall sky region ($22.5^h < \alpha < 03^h$) which matched our available observing time. Of the 21 galaxies, 14 galaxies have $g - r < 0.6$ mag (dashed black line in Figure 1), sufficiently blue to be considered as the final targets for our 3 nights in late-September 2015. Unfortunately, only 50% of the total time was useful for observations because of stormy and cloudy conditions; we ultimately observed 9 galaxies. Comparing with the 14 prepared targets (magenta lines), the observed 9 galaxies (red) are generally consistent in distributions of $\mu_0(B)$, magnitude, color, and B/T as shown in Figure 1(c)–(f). Furthermore, comparing with the entire EGIS- α .40 LSBG sample (black), these 9 galaxies (red) sample almost the full range in $\mu_0(B)$ from 22.5 to 24.5 mag arcsec $^{-2}$, but they sample only the fainter part in r ($\gtrsim 15.5$ mag) and only the blue part in $g - r$ (< 0.6 mag).

On the other hand, in February 2015, we had already spectroscopically observed in a similar way several galaxies (not confined to be LSBGs) in the EGIS- α .40 catalog, but with a different telescope using spare time from another program. From these objects, there are 3 galaxies with $\mu_0(B) > 22.5$ mag arcsec $^{-2}$. We overplot them (blue) in Figure 1 and find that they are comparable to our observed (Fall 2015) 9 LSBGs in distributions of main properties. So, we add these 3 LSBGs into our 9-galaxy LSBG sample in order to enlarge the overall observed sample in this paper.

We display the SDSS images of the 12 edge-on LSBGs in Figure 2 and list their main properties in Table 1. Statistically, $\mu_0(B)$ values of the 12 LSBGs range from 22.6 to 24.4 mag arcsec $^{-2}$. There is one object (AGC 228010; see Figure 2) with $h/z = 10.08$; it is a super-thin disk galaxy, previously defined to have an axial ratio between the disk scale length (h) and the scale height (z_0) in the g band larger than 10.0 (van der Kruit 1981, 1988; van der Kruit et al. 2001; de Grijs 1998). Additionally, our 12 galaxies have little (or no) optical bulges or central light concentrations, with $B/T < 0.08$ in the SDSS r band,

but they are not the only ones with $B/T < 0.08$ (see Figure 1(f)).

3. Observations

3.1. Overview

Long-slit spectroscopy of three LSBGs in the Spring sky were obtained on 2015 Feb. 18 UT with the Kast double spectrograph (Miller & Stone 1993) at the Cassegrain focus of the 3-m Shane telescope at Lick Observatory. A long slit $2''$ wide was positioned along the major axis of each target, and the seeing was $\sim 1.5''$. For the blue side, a 452 lines mm^{-1} grating blazed at 3306 \AA was used in first order, yielding a wavelength range of $3150\text{--}6300 \text{ \AA}$ with a spectral resolution of $1.41 \text{ \AA pixel}^{-1}$. Use of a dichroic allows simultaneous observations at longer wavelengths with the red side; however, Lick spectroscopy was obtained only with the blue side.

The other nine LSBGs were observed on 2015 Sep. 21 UT (seeing $1.5''$) and Sep. 23 UT (seeing $1.2''$) with the 5-m Hale telescope at Palomar Observatory. We used the Double Spectrograph (DBSP; Oke & Gunn 1982) and a $128''$ -long slit of width $2''$, positioned along the major axis of each target. A D68 dichroic was used to divide the wavelength coverage into two regions, $3671\text{--}6727 \text{ \AA}$ for the blue side (600 lines mm^{-1} grating blazed at 4000 \AA) and $6223\text{--}9577 \text{ \AA}$ for the red side (600 lines mm^{-1} grating blazed at $10,000 \text{ \AA}$). The respective spectral resolutions are $1.078 \text{ \AA pixel}^{-1}$ and $0.819 \text{ \AA pixel}^{-1}$, so both gratings resolve all possible line features of interest to us.

The total exposure times at Lick and Palomar for a galaxy were $3600\text{--}7200 \text{ s}$, subdivided into 2–4 subexposures in order to remove cosmic rays and enhance the signal-to-noise ratio (S/N) of the combined spectra. See Table 2 for a log of observations.

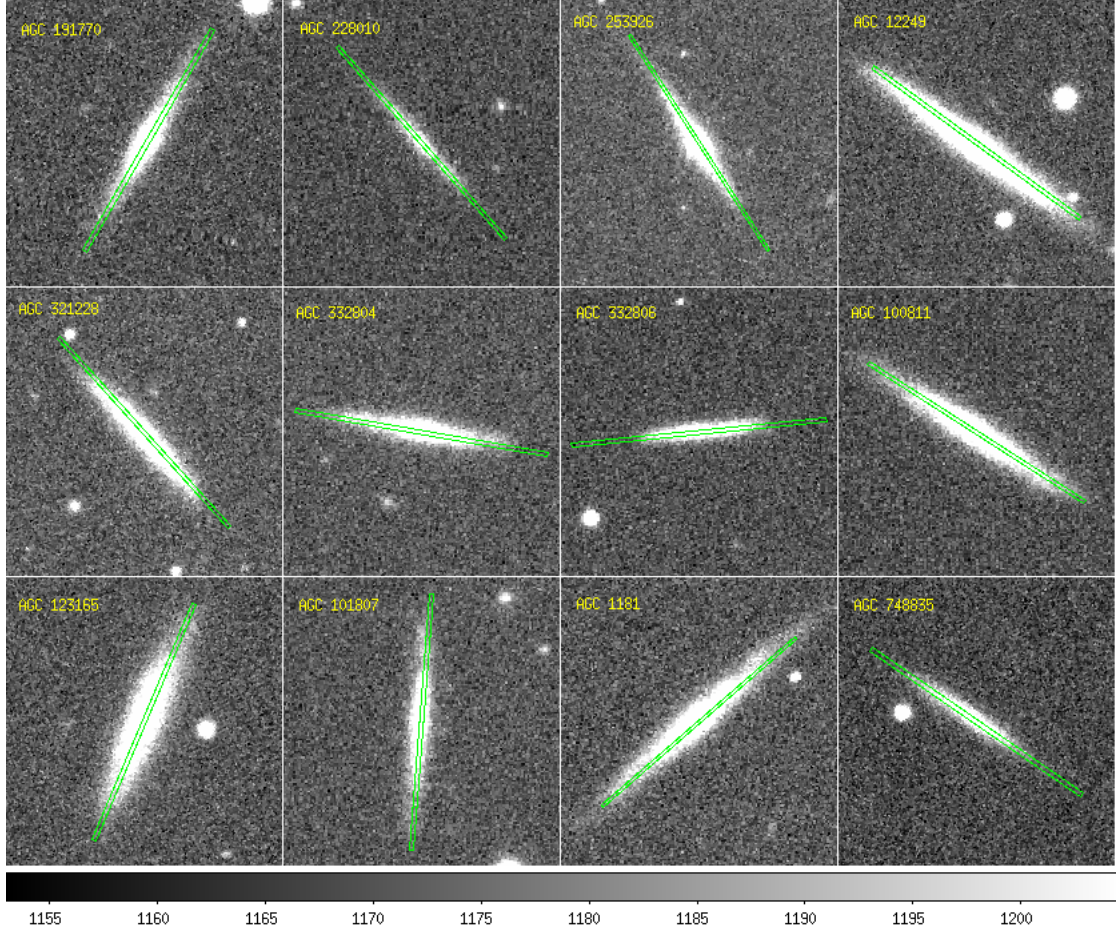


Fig. 2.— Schematic diagram of the positioning of the long slit when observing our 12 edge-on LSBGs.. In each panel, north is at top and east is to the left. The slit is indicated with a narrow green box which is scaled to the size of the slit of width 2'' and length 128''.

Table 1. Properties of Edge-on LSBGs Taken from the EGIS- α .40 Sample

Name	α (J2000) (deg) PA (deg)	δ (J2000) (deg) B/T^c	v_{helio}^a (km s $^{-1}$) $\log(M(\text{H I})/M_{\odot})$	Distance (Mpc) W_{50} (km s $^{-1}$)	$\mu_0(B)^b$ (mag arcsec $^{-2}$) S_{21} (Jy km s $^{-1}$)	g (mag)	r (mag)	h (arcsec)	z (arcsec)
191770	145.940 149.97	14.680 0.06	3823 9.07	57.4 165	23.27 1.50	17.21	16.88	6.04	1.60
228010	194.909 41.12	6.446 0.04	6354 9.45	95.3 165	24.31 1.32	17.90	17.63	10.39	0.96
253926	227.023 32.85	6.863 0.08	9333 10.26	135.9 264	23.33 4.19	17.05	16.46	6.55	1.55
12249	343.834 53.80	28.346 0.05	7549 9.73	102.9 295	23.59 2.15	16.08	15.52	11.87	1.93
321228	344.597 42.00	26.028 0.06	7492 9.26	102.1 104	22.84 0.75	16.92	16.39	5.92	1.71
332804	354.608 80.07	15.941 0.06	12425 9.99	172.3 266	23.16 1.40	16.91	16.43	6.85	1.65
332806	354.807 95.95	15.697 0.05	12055 9.83	167.0 242	22.88 1.03	17.33	17.04	4.24	1.05
100811	3.981 57.34	16.004 0.06	8362 9.77	114.4 239	23.67 1.89	16.38	15.88	10.44	2.12
123165	39.174 157.24	28.784 0.07	4536 8.95	61.9 205	22.68 0.99	16.1500	15.65	7.68	2.83
101807	14.957 175.54	14.328 0.04	11916 10.1	165.6 308	24.40 1.97	17.13	16.63	9.37	1.43
1181	25.125 130.95	14.523 0.06	8133 9.93	112.0 292	23.31 2.89	16.34	15.89	10.19	2.20
748835	31.840 55.53	15.429 0.04	12793 9.96	178.9 266	23.37 1.22	17.69	17.10	5.41	1.20

^aRadial velocity from Haynes et al. (2011).^b B -band central surface brightness from Bizyaev et al. (2014).^cBulge-to-total luminosity ratio of the galaxy from the SDSS catalog.

3.2. Light-Loss Problem

The atmosphere is a dispersive medium. At nonzero zenith angles, a stellar image will be spread out into a small spectrum, and this spread can be significant compared to the size of the seeing disk. Under these conditions, if the spectrograph slit is not oriented along the direction of atmospheric dispersion (the parallactic angle), starlight at some wavelengths will not enter the narrow slit, while starlight at other wavelengths will pass into the instrument relatively unhindered.

During our observations, the slit was actually oriented along the major axis of the target object (position angle) instead of the parallactic angle, and the object was centered in the slit at $\sim 6000 \text{ \AA}$. Therefore, at nonzero zenith angles, object light from either wavelength end (blue or red) may be selectively lost. For example, as seen in Table 2, the spectrum of AGC 191770 at airmass 1.08 was obtained with a $128'' \times 2''$ slit on a night when the seeing was $1.5''$. Then, following the calculations of Filippenko (1982), if AGC 191770 was centered in the slit at a wavelength of 6000 \AA , it would be off center by $0.61''$ at 3600 \AA ($R_{\lambda 3600}$) and by $0.05''$ in the opposite direction at 6500 \AA ($R_{\lambda 6500}$). The parallactic angle was 3.05° east of north, but the slit was actually aligned along a position angle of 149.97° east of north. So, if AGC 191770 was a star with a Gaussian point-spread function, the percentage of light entering the slit at 3600 \AA ($T_{\lambda 3600}$), 6000 \AA ($T_{\lambda 6000}$), and 6500 \AA ($T_{\lambda 6500}$) would be (respectively) 83.5, 88.3, and 88.3. Thus, the light loss at 3600 \AA would be 4.8% greater than that at 6000 \AA .

Differential losses are a bigger concern for point sources than for extended objects such as galaxies. For extended sources, especially if the surface brightness is roughly constant over an area larger than the slit width, blue-end light loss from the position being observed can be partly gained back from neighboring positions within the source. The effect on the relative flux calibration will not be very large for our targets because of the following

reasons. (1) Most spectra of our targets were observed at small airmasses (Table 2). (2) Our targets are edge-on galaxies with extended areas larger than the slit width (see Figure 2), so the blue and red light losses are partly gained back from the neighboring positions within the objects. For completeness, we do the calculations above for all our targets (at the midpoint of the exposures) and list the results in Table 2.

Table 2. Log of Observations of Edge-on LSBGs

Name	UT Date YYYY-MM-DD	Exp. (s)	blue λ range (\AA)	red λ range (\AA)	Tel. & Instr.	airmass	Position Angle deg (East of North)
	Parallactic Angle deg (East of North)	$R_{\lambda 3600}$ arcsec	$R_{\lambda 6000}$ arcsec	$R_{\lambda 6500}$ arcsec	$T_{\lambda 3600}$ %	$T_{\lambda 6000}$ %	$T_{\lambda 6500}$ %
191770	2015-02-18	2×2700	3450–6450		Shane Kast	1.080	149.97
	3.05	0.61	0.00	-0.05	83.5	88.3	88.3
228010	2015-02-18	2×3600	3450–6450		Shane Kast	1.170	41.12
	143.88	0.80	0.00	-0.06	63.0	88.3	88.2
253926	2015-02-18	2×2400	3450–6450		Shane Kast	1.170	32.85
	24.11	0.80	0.00	-0.06	87.7	88.3	88.3
12249	2015-09-21	3×1200	3671–6727	6223–9577	Hale DBSP	1.239	53.80
	108.52	0.91	0.00	-0.08	65.8	95.0	94.9
321228	2015-09-21	4×1200	3671–6727	6223–9577	Hale DBSP	1.027	42.00
	125.96	0.97	0.00	-0.08	52.7	95.0	94.8
332804	2015-09-21	3×1200	3671–6727	6223–9577	Hale DBSP	1.048	80.07
	177.59	0.42	0.00	-0.03	87.0	95.0	94.9
332806	2015-09-21	4×1200	3671–6727	6223–9577	Hale DBSP	1.055	95.95
	18.51	0.47	0.00	-0.04	85.6	95.0	94.9
100811	2015-09-21	4×1200	3671–6727	6223–9577	Hale DBSP	1.117	57.34
	45.41	0.67	0.00	-0.05	94.2	95.0	95.0
123165	2015-09-21	3×1200	3671–6727	6223–9577	Hale DBSP	1.016	157.24
	61.13	0.27	0.00	-0.02	91.9	95.0	95.0
101807	2015-09-23	3×1200	3671–6727	6223–9577	Hale DBSP	1.057	175.54
	0.38	0.47	0.00	-0.04	94.9	95.0	95.0
1181	2015-09-23	3×1200	3671–6727	6223–9577	Hale DBSP	1.062	130.95
	16.35	0.47	0.00	-0.04	86.7	95.0	94.9
748835	2015-09-23	3×1200	3671–6727	6223–9577	Hale DBSP	1.088	55.53
	37.02	0.57	0.00	-0.04	93.6	95.0	95.0

4. Data Reduction

4.1. Overview

Data reduction was carried out using standard IRAF procedures. After correction for overscan, bias, and flat field, we reject cosmic rays using the IRAF task L.A.Cosmic (van Dokkum et al. 2001), which identifies and removes cosmic rays robustly from astronomical images via a Laplacian algorithm. Then, we performed wavelength calibration on the two-dimensional (2D) spectral images of objects and standard stars. Sky subtraction will be described more detailedly in next subsection. After sky subtraction, we defined the appropriate aperture, traced the flux peaks along the dispersion direction, and interactively extracted one-dimensional (1D) spectrum by using the APALL task of IRAF. Finally, we averagely combined spectra from multiple exposures for an object into one final spectrum.

In Figure 3, we show the combined blue-side spectra for the three galaxies observed with the Lick Shane telescope (they have no red-side observations). For the nine galaxies observed with the Palomar Hale telescope, both the blue- and red-side spectra are shown (with blue and red colors, respectively), after scaling the red side to match the flux level of the blue side in the small overlap region. Strong emission lines are marked. Generally, the night-sky lines are not clearly subtracted in the faint LSBG spectra, so we simply mask four wavelength regions having the strongest night-sky lines (green).

4.2. Sky Subtraction

Sky subtraction quality is very important for LSBGs as they are naturally fainter than the sky background in surface brightness. So, we describe the three methods of sky subtraction we have tried in data reduction for our observations below.

The first one is called the “median-filter method.” Before performing this method, we make the spatial and dispersion directions perpendicular to each other through rectification, such as by performing 2D wavelength calibration on spectral images of objects. Then, on the rectified images, assuming the direction of night-sky lines is along the column, we perform a median filter represented by a $1 \times n$ array along each column to generate a sky image. Here, n must be larger than at least two times the width (major axis in pixels) of the object projected on the images. This method is good at removing sky lines but may overestimate the sky continuum blended in the object.

The second one is the sky-fitting method adopted in the APALL task of IRAF, which uses a second-order polynomial to fit the background from the substantial sky region along the slit. This method can do well in estimating sky continuum blended in the object but does not do very well in removing sky lines.

The third one is the Kelson (2003) method which makes full use of the raw image data (before the optical distortions and spectral line curvatures have been rectified) to model the sky background. This method is not very good for our faint objects, because it either underestimates the sky continuum or leaves sky-line residuals in our images.

None of the three methods above is sufficiently good at removing both sky continuum and sky lines clearly from spectra of our faint LSBGs. However, we have no other good ideas to implement it ideally. So, for Lick data which have no obvious distortions of raw images, the first “median-filter” method has been used to simultaneously subtract the sky lines and sky continuum. However, for Hale data which have relatively serious distortions of raw images, this “median-filter” method does not do well in sky continuum subtraction, so we finally used the second method to improve the sky continuum subtraction a little better, but we warn the reader that the final spectral continuum shapes for Hale spectra are still probably not accurate.

4.3. Problems in the Spectra

Examining the extracted spectra, it appears that the reductions of the Hale spectra are not good at wavelengths $< 3800 \text{ \AA}$. Unexpectedly, many absorption lines appear in the observed spectra of our standard stars in this blue-end region due to unresolved reasons, so we are not able to determine an accurate continuum shape for fitting the flux-calibration curve in this blue-end region. Fortunately, except for AGC 123165, our LSBG galaxies all have redshift $z > 0.02$, so the bluest useful line ([O II] $\lambda 3727$) falls at $\lambda > 3800 \text{ \AA}$.

Although we have extracted the red-side Palomar Hale spectra, their continuum S/N is quite low, so we abandoned using the red-side spectral continuum. However, the emission lines in the red spectra, such as [N II] $\lambda 6584$, $H\alpha$, and [S II] $\lambda\lambda 6716, 6731$, are reasonably strong, and they could therefore be used for dust-extinction corrections and oxygen-abundance measurements.

Moreover, as mentioned above, the spectral continuum shapes of the nine galaxies observed with the Hale telescope are not reliable, so we will not use them to draw any firm conclusions.

5. Results

5.1. Oxygen Abundance

The gas-phase metallicity (oxygen abundance, $Z = 12 + \log(\text{O}/\text{H})$) of a galaxy is a powerful probe of the past star formation and growth. It can also constrain the current stage of galaxy evolution as it is intimately connected to the fueling and regulation of star formation. Usually, flux ratios of strong optical emission lines are used as the abundance-sensitive diagnostics, such as R_{23} , [N II]/[O II], [N II]/ $H\alpha$, [N II]/[S II], and so

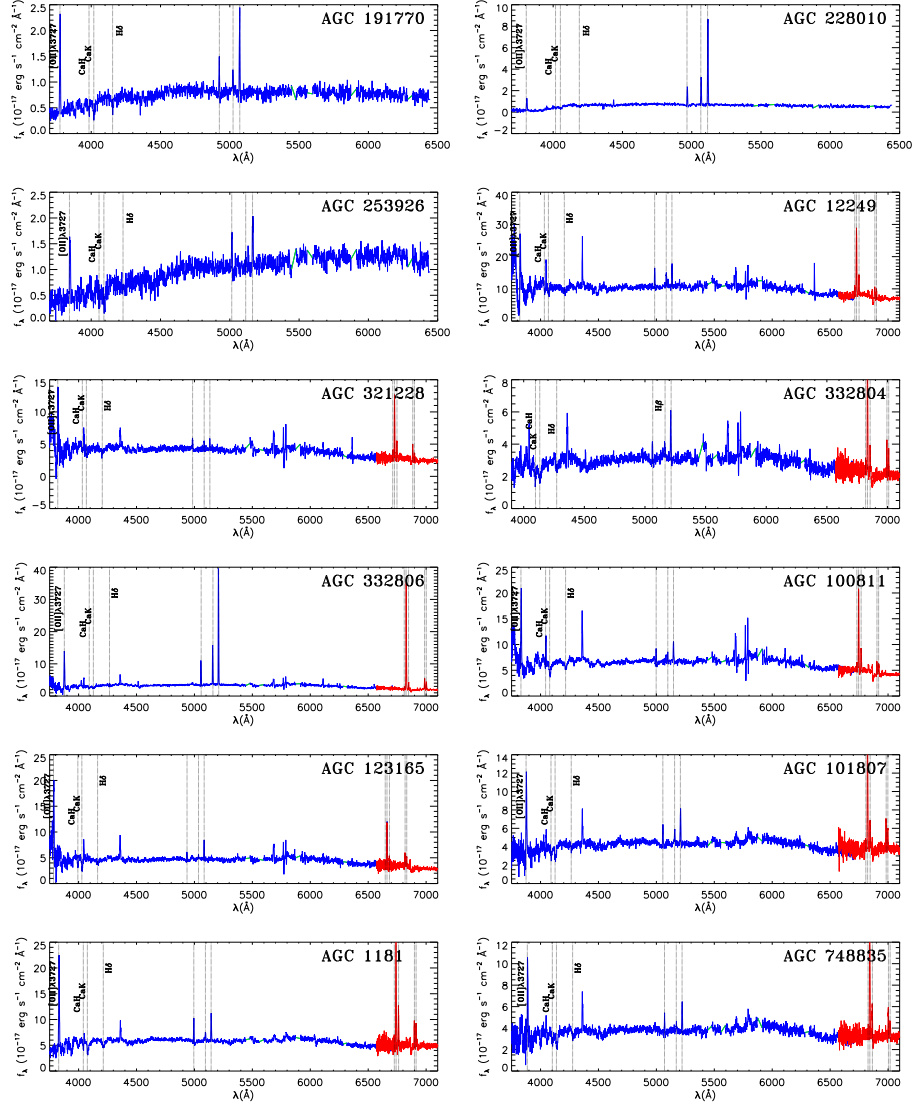


Fig. 3.— Spectra of 12 edge-on LSBGs . The blue- and red-side spectra from Lick (blue only; first 3 objects) and Palomar (next 9 objects) are shown in blue and red, respectively. The red-side spectrum is scaled to the flux level of the blue-side spectrum by using the wavelength region of overlap; the scale factors are ~ 1.2 . Here, we show only spectra at $\lambda > 3700 \text{ \AA}$ and (for the Palomar data) $\lambda < 7100 \text{ \AA}$. This region contains the emission lines used in this study.

on (Pagel et al. 1979; Kewley & Dopita 2002). Based on extracted spectra of our LSBGs, we measure the observed fluxes of strong emission lines in the blue-side ($[\text{O II}] \lambda 3727$, $\text{H}\beta$, $[\text{O III}] \lambda\lambda 4959, 5007$) and red-side ($[\text{N II}] \lambda\lambda 6548, 6584$, $\text{H}\alpha$, $[\text{S II}] \lambda\lambda 6716, 6731$).

An intrinsic $\text{H}\alpha/\text{H}\beta$ flux ratio of 2.86 is assumed for Case B recombination at 10^4 K (Osterbrock 1989) because the relative intensities of the hydrogen Balmer lines are nearly independent of density and temperature. Therefore, for observed line fluxes measured from the 9 Hale spectra which have both blue- and red-side, we use the Balmer decrement ($\text{H}\alpha/\text{H}\beta$) and the CCM extinction law with $R_V = 3.1$ (Cardelli et al. 1989) to correct dust extinction. Based on these intrinsic fluxes, we compute several useful flux ratios of $[\text{N II}]/[\text{O II}]$, $[\text{N II}]/[\text{O III}]$, $[\text{N II}]/\text{H}\alpha$, and R_{23} [where $R_{23} = ([\text{O II}] \lambda 3727 + [\text{O III}] \lambda\lambda 4959, 5007)/\text{H}\beta$], among which $[\text{N II}]/\text{H}\alpha$ and R_{23} are individually used as metallicity diagnostics. For the $[\text{N II}]/\text{H}\alpha$ diagnostic, both the PP04 (Pettini & Pagel 2004) and D02 (Denicolo et al. 2002) calibrations are used to measure the oxygen abundances. For the R_{23} diagnostic, both the M91 (McGaugh 1991) and Z94 (Zaritsky et al. 1994) calibrations are employed to measure the oxygen abundances. Thus, we have four sets of oxygen abundances for each of the 9 Hale-observed galaxies except for AGC 123165 which have no R_{23} -based metallicities because its spectra has some problem in the blue-end wavelength range covering $[\text{O II}] \lambda 3727$ (see §4.3). It should be noted that when using the M91 calibration, we need to determine which branch is appropriate for each galaxy because the R_{23} versus O/H relation is double-valued (Kewley & Dopita 2002; de Naray 2004). Distinguishing a branch (high- Z or low- Z) can be accomplished with the $[\text{N II}] \lambda 6584$ line: strong (weak) nitrogen emission indicates that the high- Z (low- Z) branch is appropriate. The dividing line is at $\log([\text{N II}]/[\text{O II}]) \approx -1.2$ (Kewley & Dopita 2002). However, for observed line fluxes measured from the 3 Lick spectra which have no observed red-side spectra (neither $\text{H}\alpha$ nor $[\text{N II}]$), no reddening correction is performed and only R_{23} diagnostic and R_{23} -based metallicities are measured. When using the M91 calibration, no available $\log([\text{N II}]/[\text{O II}])$

can be used for distinguishing branches, so we empirically adopt the low- Z branch to measure metallicities as LSBGs are generally acknowledged to be metal-poor.

In Table 3, we report measurement results above and also show the average (Z_{ave1}) of both R_{23} -based metallicities (Z_{Z94} and Z_{M91}) and the average (Z_{ave2}) of both $[\text{N II}]/\text{H}\alpha$ -based metallicities (Z_{PP04} and Z_{D02}) for each LSBG. In statistic, our measurements show that the R_{23} -based metallicities (Z_{ave1}) are 8.00–8.62 dex, with a mean of 8.30 dex and a median of 8.26 dex. The $[\text{N II}]/\text{H}\alpha$ -based metallicities (Z_{ave2}) are 7.67–8.54 dex, with a mean of 8.20 dex and a median of 8.26 dex. Generally, the two sets of metallicities are consistent with each other and are both subsolar, with the $12 + \log(\text{O}/\text{H})$ value being 8.87 dex for the Sun (Grevesse et al. 1996). Our metallicities for the LSBG sample agree with the results for LSBGs from de Naray (2004) (see Figure 4).

5.2. The Luminosity-Metallicity Relation

The strong correlation between galaxy luminosity (L) and galaxy metallicity (Z) is one of the most significant phenomenological results in chemical evolution studies of galaxies. Previous work found that the correlations between L and Z for irregular galaxies (Lequeux et al. 1979; Skillman et al. 1989), disk galaxies (predominantly high surface brightness galaxies, HSBGs; Garnett et al. 1987), and elliptical galaxies (Faber 1973; Brodie & Huchra 1991) are very similar. Thus, it is instructive to plot our LSBG sample onto the familiar L – Z relation defined by previous work on other galaxy types to validate the consistency of our measurements of LSBGs.

In the L – Z plot in Figure 4, we show both R_{23} -based (red filled circles) and the $[\text{N II}]/\text{H}\alpha$ -based (black filled circles) metallicities for our LSBGs. Here, the B -band absolute magnitude for our LSBGs are computed from the galaxy distances (provided by $\alpha.40$

Table 3. Emission-Line Ratios^a and Oxygen Abundance of Edge-on LSBGs

AGC No.	$(\text{H}\alpha/\text{H}\beta)_{\text{obs}}$	$\log([\text{N II}]/[\text{O II}])$	R_{23}	$\log([\text{N II}]/\text{H}\alpha)$	Z_{M91}	Z_{Z94}	Z_{PP04}	Z_{D02}	$Z_{\text{ave1}}^{\text{b}}$	$Z_{\text{ave2}}^{\text{c}}$
191770			5.93		8.04	8.68			8.36	
228010			6.64		7.80	8.59			8.195	
253926			4.16		7.78	8.89			8.335	
12249	3.42	-0.67	5.98	-0.70	8.56	8.67	8.46	8.61	8.615	8.535
321228	4.67	-1.10	11.44	-1.13	8.00	8.01	8.22	8.30	8.005	8.26
332804	5.79	-1.30	13.00	-1.36	8.79	7.85	8.14	8.13	8.32	8.135
332806	3.53	-0.98	7.63	-2.07	8.53	8.47	7.72	7.61	8.5	7.665
100811	4.19	-0.92	9.37	-0.94	8.22	8.27	8.31	8.44	8.245	8.375
123165	6.24			-1.08			8.24	8.33		8.285
101807	4.55	-1.05	9.35	-1.51	8.24	8.27	8.08	8.02	8.255	8.05
1181	5.30	-1.01	9.89	-1.14	8.15	8.21	8.22	8.29	8.18	8.255
748835	4.76	-1.04	9.37	-1.18	8.20	8.27	8.20	8.26	8.235	8.23

^aCorrected for reddening.

^a Z_{ave1} is the average value of Z_{M91} and Z_{Z94} , which are both based on the R_{23} diagnostic.

^b Z_{ave2} is the average value of Z_{PP04} and Z_{D02} , which are both based on the $[\text{N II}]/\text{H}\alpha$ diagnostic.

catalog) and the B -band apparent magnitudes (which are transformed from magnitudes of g - and r -bands measured by our own surface photometry (Du et al. 2015)). Data of LSBGs from de Naray (2004) (purple triangles) and dwarf irregulars (dIrrs; dark-green squares) from Lee et al. (2003) are also plotted in this L – Z figure for comparisons. Besides, we show a variety of recent fits to the L – Z relation determined respectively for the dIrr sample of Lee et al. (2003) (green line), a large sample of SDSS star-forming galaxies from Tremonti et al. (2004) (orange line), a large sample of starbursting emission-line galaxies drawn from the KISS (KPNO International Spectroscopic Survey) sample from Melbourne & Salzer (2002) (cyan line), and a large sample of 2dFGRS (Two-Degree Field Galaxy Redshift Survey) star-forming galaxies from Lamareille et al. (2004) (blue line) from the literature. Among these relations, it seems that there is some disparities, which are probably caused by the utilization of different samples and different diagnostics and calibrations for measuring abundances.

It is not easy to constrain a quantitatively reliable L – Z relation for our LSBG data; they do not have sufficient leverage because of their small coverage in luminosity space. As shown in Figure 4, if all 12 galaxies (red filled circles) are considered, our sample covers only ~ 3 mag of absolute magnitude, and if only the 9 galaxies (black filled circles) having both blue- and red-side spectra are considered, it covers only ~ 1 mag. Instead of being quantitative, we thus carry out our studies qualitatively. From Figure 4, it appears that our LSBG sample with both sets of metallicities, especially with the $[\text{N II}]/\text{H}\alpha$ -based metallicities, seems to generally follow the similar distribution as the LSBGs from de Naray (2004) in their common covering region in luminosity and metallicity space. Both LSBG samples are consistent with the general distribution trend of other samples (normal galaxies, dIrrs) in this L – Z plot, although with some degree of scatter.

Additionally, we checked for quantitative consistency between our sample and the

LSBG sample from de Naray (2004). We did the test 50 times. Each time, we randomly picked a subsample of size equal to our small LSBG sample with $[\text{N II}]/\text{H}\alpha$ -based metallicities from the LSBG sample of de Naray (2004), and then checked to see whether this subsample gives a distribution consistent with our small LSBG sample by using a K-S test. Our criteria for each K-S test to decide whether the subsample is consistent with being drawn from the same distribution as our small LSBG sample is the probability value being larger than 0.90 ($P > 0.90$). The result is that in the total of 50 trials, 32% of the subsamples from the de Naray (2004) LSBG sample give distributions that are consistent with our limited LSBG sample in the L – Z plot. Any fraction more than 10% and less than 90% is basically inconclusive. So, such a fraction shows that the samples are too small to provide a conclusive result. If our sample could be improved to a larger size and wider luminosity coverage, such quantitative tests might give a more conclusive statistical fraction for consistency.

5.3. The Mass-Metallicity Relation

5.3.1. Stellar Mass Estimate

For our LSBGs, we derived two sets of stellar masses. One set is the “ B -based” stellar masses which are derived by using their B -band luminosity and $B - V$ color transformed from $g - r$ measured in (Du et al. 2015). The other set is the “ z -based” stellar masses in the SDSS MPA-JHU catalog which are computed from the SDSS z -band luminosities in synergy with the z -band stellar M/L derived by the SDSS multi-band SED fitting method (Kauffmann et al. 2003). Resultantly for our LSBGs, the “ B -based” stellar masses are $M_{\star} \approx 10^{7.89-10^{9.21}} \text{ M}_{\odot}$, with a mean of $10^{8.81} \text{ M}_{\odot}$ and a median of $10^{9.09} \text{ M}_{\odot}$. The “ z -based” stellar masses are $10^{8.37-10^{9.96}} \text{ M}_{\odot}$, with a mean of $10^{9.42} \text{ M}_{\odot}$ and a median of $10^{9.79} \text{ M}_{\odot}$. We report the results in Table 4. Apparently, the set of “ B -based” stellar masses is on

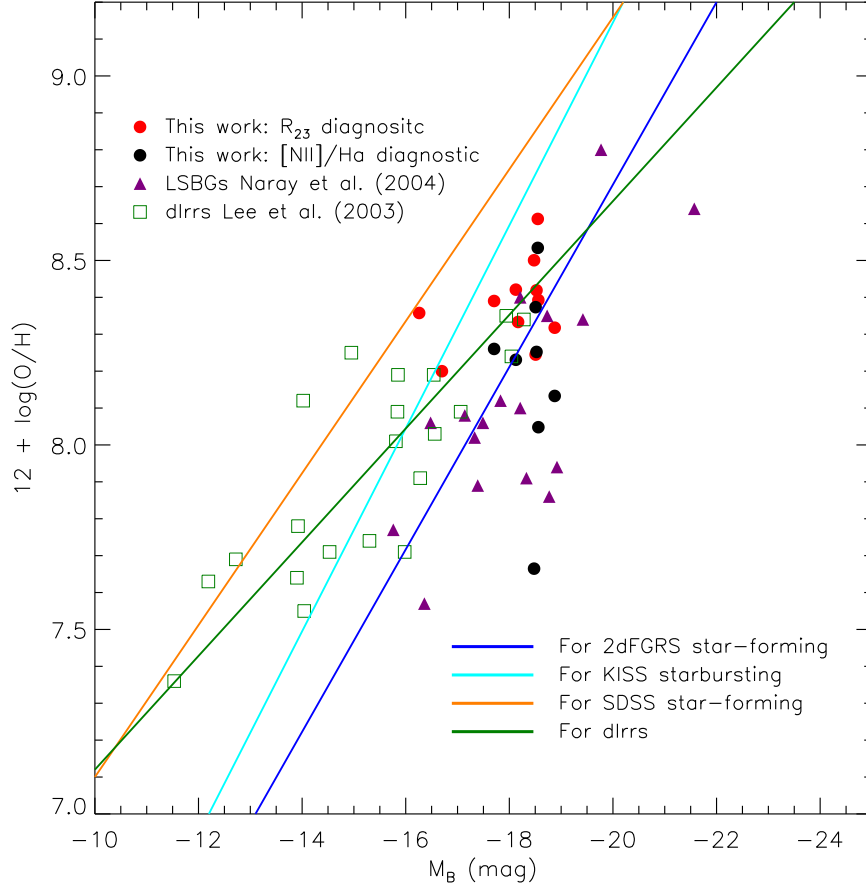


Fig. 4.— Luminosity-metallicity plot for our LSBG sample. The red and black filled circles respectively refer to the R_{23} -based and $[\text{N II}]/\text{H}\alpha$ -based metallicities. The purple triangles refer to the LSBG sample of de Naray (2004). The green squares are the dwarf irregular galaxy sample of Lee et al. (2003). The blue solid line is the fitted L – Z relation from Lamareille et al. (2004), which is determined for a large sample of 6387 star-forming galaxies in the local universe ($0 < z < 0.15$) from the 2dFGRS. The orange solid line is the relation determined by Tremonti et al. (2004) for a large sample of 53,000 star-forming galaxies at $z \approx 0.1$ from the SDSS. The cyan solid line is the relation of Melbourne & Salzer (2002) for a large sample of ~ 900 starbursting emission-line galaxies from KISS. The dark-green solid line is the relation for the dIrr sample (dark-green squares) of Lee et al. (2003).

average ~ 0.6 order of magnitude lower than the set of “ z -based” stellar masses. In this paper, we prefer the “ z -based” stellar masses for our LSBGs, and the reason will be given in §6.2.

5.3.2. M – Z plot

We show our LSBG data in the mass-metallicity (M – Z) plot in Figure 5. For metallicity, both R_{23} -based (black) and $[\text{N II}]/\text{H}\alpha$ -based (red) oxygen abundances are displayed. For stellar mass, both the “ B -based” (open circles) and “ z -based” (filled circles) stellar masses are shown. So, in this M – Z plot, our LSBG sample appears as four individual sets of distributions, among which the two sets represented by red and black open circles are systematically biased to lower stellar mass because the “ B -based” stellar masses may be underestimated (as mentioned in §5.3.1 and discussed in §6.2). So, comparing with distributions represented by the red and black open circles, we prefer distributions based on the “ z -based” stellar mass estimations (red and black filled circles). For comparison, the LSBG sample (purple triangles) of de Naray (2004), the dIrr sample (dark-green squares) of Lee et al. (2003), and the massive spiral galaxy sample (brown asterisks) of Garnett et al. (1987) in the very local universe (including M101, M31, NGC 1365, M81, NGC 2997, and so on) are also included in this M – Z plot. Additionally, the M – Z relation determined for $\sim 53,400$ SDSS star-forming galaxies of Tremonti et al. (2004) is shown. The black open diamonds represent the median in bins of 0.1 dex in stellar mass that include at least 100 data points. The magenta line shows the polynomial fit of Tremonti et al. (2004) to the median data. The cyan blue dashed and solid lines are the contours that enclose 68% and 95% of the data.

Obviously, the distributions of our LSBG sample with “ z -based” stellar mass are generally consistent with the LSBG sample from de Naray (2004) at their common stellar

mass space. Additionally, for normal star-forming galaxies and other types, there is a tendency that galaxies with lower stellar masses generally have lower metallicities. Specifically, for normal star-forming galaxies with stellar masses between $10^{8.5}$ and $10^{10.5}$ M_{\odot} , Tremonti et al. (2004) find the correlation between stellar mass and metallicity to be roughly linear. Owing to the small coverage in stellar mass space, our LSBG sample is not sufficient for fitting a certain $M-Z$ relation, but galaxies in our sample are consistent with the relatively low abundances for their stellar masses.

5.4. The Gas Mass Fraction vs. Oxygen Abundance

The gas consisting mostly of hydrogen and helium is the raw material out of which stars and metals are formed. In LSBGs, the largest constituent of gas is assumed to be neutral atomic hydrogen. The molecular gas remains unknown in quantity but, fortunately, it is not expected to contribute greatly to the total mass of gas in LSBGs due to their low metallicities and low dust content (Schombert et al. 1990; de Blok 1998). As for ionized gas, it contributes negligibly to the mass of LSBGs (Schombert et al. 2001).

The gas mass fraction (f_g) refers to the fraction of baryons in gaseous form. It can be simply measured by the ratio of the total mass in gas (M_{gas} , including molecular, atomic, ionized, and metals) to the combined total mass in gas and stars (M_{\star}):

$$f_g = \frac{M_{\text{gas}}}{M_{\text{gas}} + M_{\star}}. \quad (1)$$

So, taking the contribution of helium and metals into account, the total gas mass of LSBGs in units of solar mass can be given by

$$M_{\text{gas}} = \frac{M_{\text{H I}}}{X}, \quad (2)$$

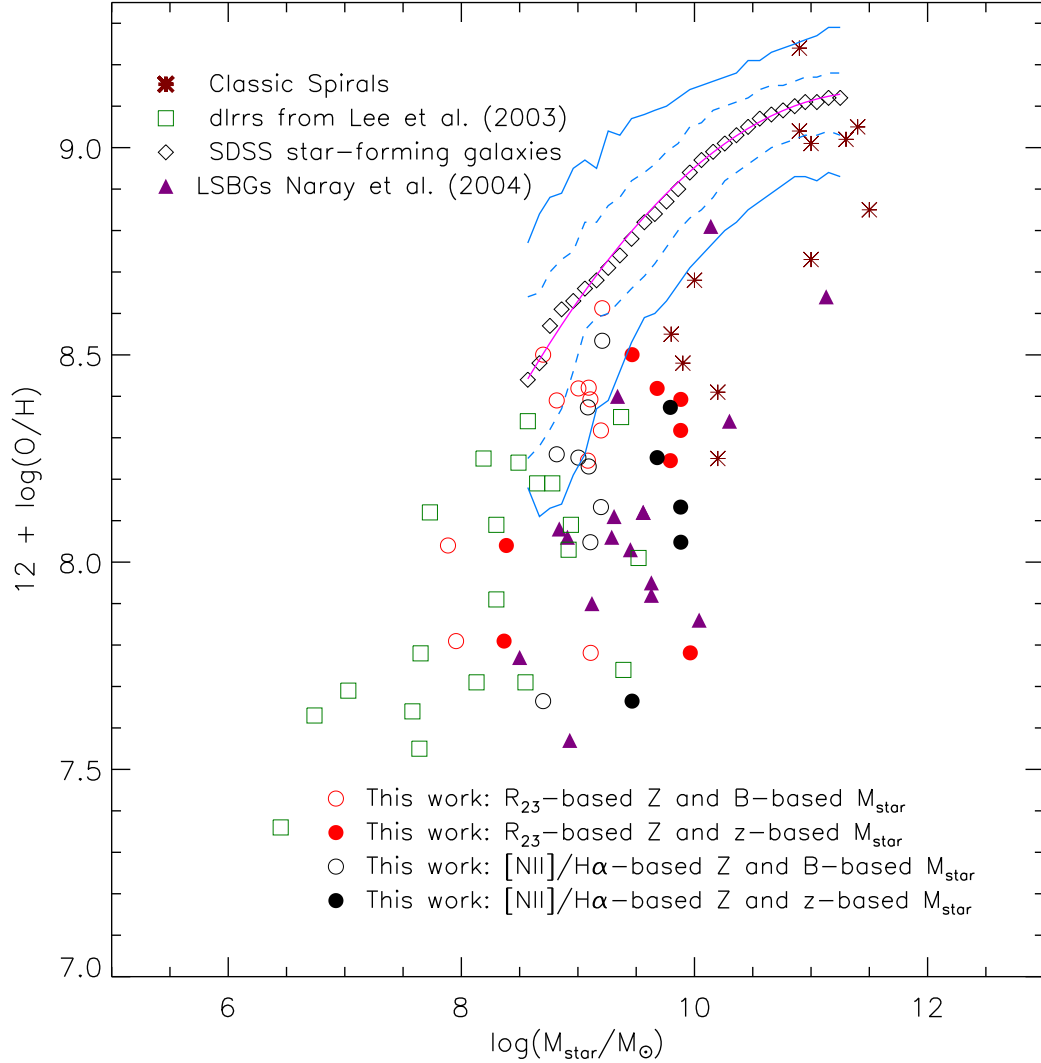


Fig. 5.— Mass-metallicity plot for our LSBG sample. Our edge-on LSBGs are shown by red or black circles, respectively representing the R_{23} -based and $[\text{N II}]/\text{H}\alpha$ -based abundances. The open and filled circles show stellar masses estimated respectively from the $B-V$ color and the SDSS SED-fitting. Purple triangles, brown asterisks, and dark-green squares stand for the LSBG sample from de Naray (2004), the normal massive spiral galaxies from Garnett et al. (1987), and the dIrr sample from Lee et al. (2003). The black open diamonds indicate the medians of the 53,000 SDSS star-forming galaxies from Tremonti et al. (2004) in bins of 0.1 dex in stellar mass, and the magenta line shows the polynomial fit to the median data from all of the bins. The cyan blue dashed and solid lines are respectively contours that enclose 68% and 95% of the 53,000 star-forming galaxies.

where X is the fraction of the gas mass in the form of hydrogen, adopted to be 0.733 (de Blok 1998).

Following the formula above, M_{gas} for our edge-on LSBG sample can be easily computed by multiplying $M_{\text{H I}}$ (Table 1) which is available from the α .40 catalog (Haynes et al. 2011) by $1/0.733$. For M_{\star} , we have previously derived two sets of stellar masses for our LSBG sample in §5.3.1 (Table 4). Consequently, we have two sets of gas mass fraction, f_g , for our sample.

In Figure 6, we show oxygen abundance versus inverse gas mass fraction for our LSBG sample. Both sets of gas mass fractions are shown for our sample. The filled circles represent for f_g being computed from the “ z -based” M_{\star} while the open circles are for f_g being computed from the “ B -based” M_{\star} . Besides, two sets of metallicities are also presented with red circles showing R_{23} -based metallicities and black circles showing $[\text{N II}]/\text{H}\alpha$ -based metallicities. For comparisons, the LSBG sample from de Naray (2004) (purple triangles) and the dIrr sample from Lee et al. (2003) (green squares) are also plotted.

For our LSBG sample, data points with “ B -based” stellar mass (red and black open circles) or with “ z -based” stellar mass but R_{23} -based metallicities (red filled circles) have systematically biased to much larger gas mass fraction, compared with other samples (e.g., the LSBG sample from de Naray 2004; the dIrr sample from Lee et al. 2003). However, data points with “ z -based” stellar mass and $[\text{N II}]/\text{H}\alpha$ -based metallicities (black filled circles) show general consistency with other samples in the common high- f_g region. The systematically larger gas mass fractions are more likely to be caused by different methods used for estimating stellar mass and metallicity. Again, we prefer the “ z -based” stellar masses for our sample because LSBGs are acknowledged to be dominated by low-mass stars that would radiate light predominantly at red and near-infrared wavelengths. Using B -band luminosity method is very likely to underestimate stellar masses of LSBGs and then

overestimate their gas mass fractions. More details on this issue will be discussed in §6.2.

6. Discussion

6.1. Stellar Populations

6.1.1. Coarse Stellar Populations Results

Stellar populations are the fossils of the past star formation and evolution of galaxies. However, the sky background makes it very difficult to study the faint stellar continuum and absorption lines in the entire LSBG unless very large telescopes and extraordinarily long exposure times are used. Because of such difficulties, most spectroscopic studies of LSBG stellar populations have been based on spectra of the brighter bulges (e.g., Morelli et al. 2012) or H II regions. A slit of appropriate width and length positioned along the major axis can generally capture light from almost all regions of an edge-on galaxy, especially of a super-thin galaxy. Thus, the spectral properties may in principle be much better determined for edge-on LSBGs compared with face-on ones.

If we expect to derive reliable stellar populations with full-spectrum fitting stellar population synthesis method, we must use high-quality spectra, especially with well-calibrated spectral continuum shapes. Given the uncertainties associated with continuum shapes of the Palomar Hale spectra, we decided to use only the three Lick Shane spectra (of AGC 191770, AGC 228010, and AGC 253926) for our stellar-population study of LSBGs. All these three spectra have $S/N > 10$ in the continuum wavelength interval 4730–4780 Å and meet our requirements.

For stellar population synthesis, STARLIGHT (Cid Fernandes et al. 2005) is a widely used tool. It can derive the age and metallicity of a galaxy, as well as its extinction and

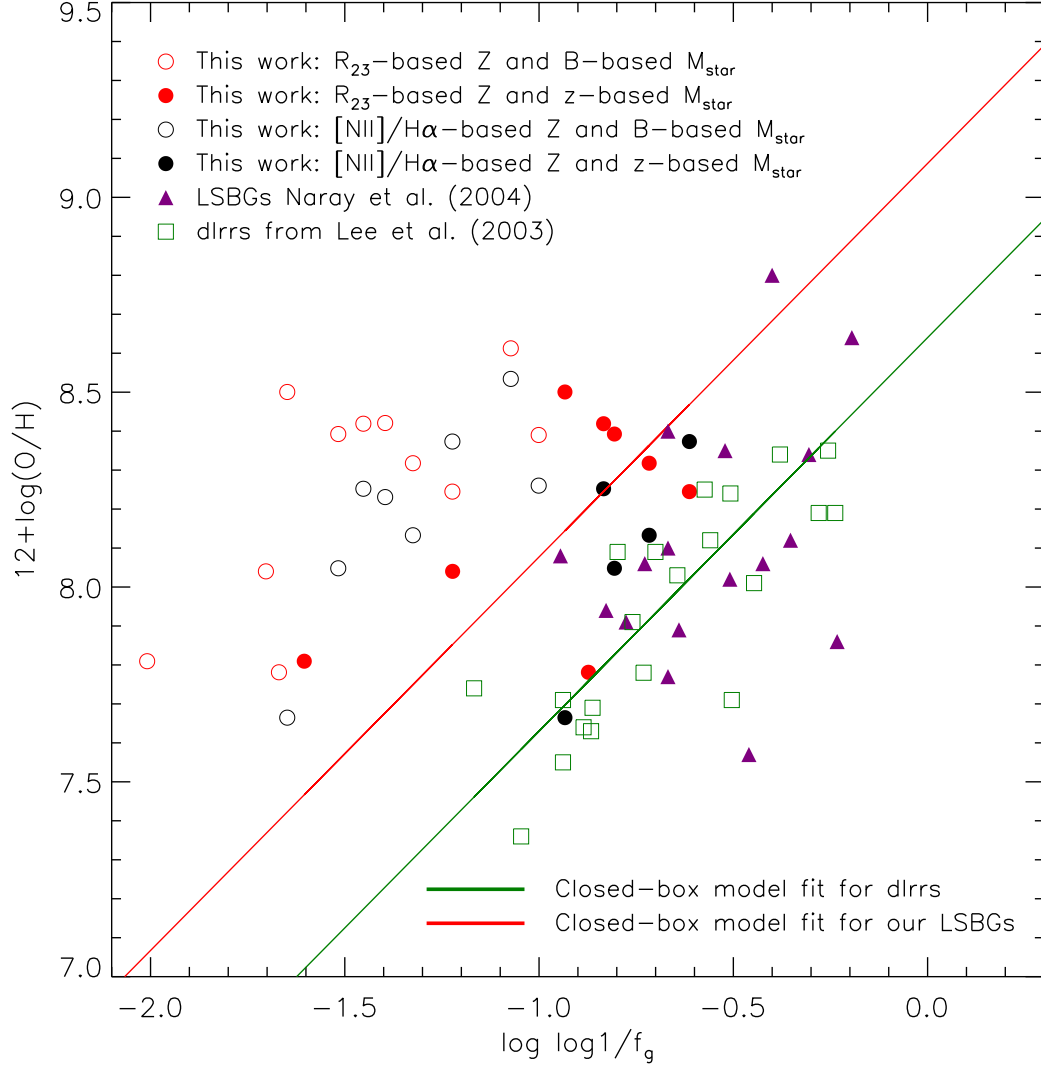


Fig. 6.— Gas mass fraction vs. metallicity for LSBGs. Different sets of stellar masses and metallicities are shown for our LSBG sample. The open and filled circles show stellar masses respectively estimated from the B -band method and the SDSS SED-fitting method, while the black and red circles respectively represent the R_{23} -based and $[NII]/H\alpha$ -based metallicities. Purple triangles and dark-green squares are respectively the LSBG sample of de Naray (2004) and the dIrr sample of Lee et al. (2003). The dark-green solid line with a slope of unity indicates the behavior of the closed-box model of chemical evolution with an oxygen yield of 2.22×10^{-3} for the dIrr sample of Lee et al. (2003). The red solid line is the ‘hypothetical’ closed-box model fit for our LSBG sample with a different oxygen yield of 6.23×10^{-3} .

velocity dispersion, by fitting its observed spectrum with a superposition of populations of various ages and metallicities from stellar population models such as STARLIGHT (Bruzual & Charlot 2003, hereafter BC03). We used STARLIGHT to perform stellar population synthesis for the integrated spectra of the three edge-on LSBGs observed at Lick. For the reddening, both the Calzetti et al. (2000, hereafter CAL) law and the Cardelli et al. (1989, hereafter CCM) law were separately used during the fit, although the problem of dust attenuation is minimal in LSBGs because they are acknowledged to be dust poor.

We show the fit plot in Figure 7. As said by Cid Fernandes et al. (2005), the individual stellar population components from STARLIGHT are very uncertain because the existence of multiple solutions is an old known problem in stellar population synthesis. Thus, we should avoid focusing in detail on any individual stellar populations. Instead, we jump straight to results based on more robust descriptions of the resultant stellar populations. As suggested in the STARLIGHT paper (Cid Fernandes et al. 2005), a coarse but robust description of the star-formation history of our galaxies may be obtained by binning the resultant individual stellar populations onto “young” (Y; age < 1 Gyr) and “old” (O; age > 1 Gyr) components. In order to show the respective contributions of the two components, we provide the “light fraction” (LF) out of the total light and the “mass fraction” (MF) out of the total mass for Y and O components in Table 5. Results from both reddening laws (CAL and CCM) for each LSBG seem to be consistent. Qualitatively, for both light and mass, the contributions from the O components seem to be much larger than those from the Y components for these three LSBGs. Thus, rather than a quantitative conclusion, we can draw a qualitative conclusion that these three LSBGs may have a potential dearth of stars with ages < 1 Gyr. Instead, they are more likely to be dominated by stars with ages > 1 Gyr. This supports the general notion that LSBGs have a very low level of current star-formation activity.

Comparing with the previously measured subsolar gas-phase metallicities for the first three galaxies in Table 3, their stellar metallicities (from stellar population synthesis; Table 5) are about solar. On one hand, this inconsistency is likely to be caused mainly by the large uncertainties of the stellar metallicities. As can be deduced from the amount of work devoted to this topic of stellar population synthesis, recovering the stellar content of a galaxy with accurately quantitative ages and metallicities from its observed integrated spectrum is not an easy task. It needs a high-quality integrated spectrum, as well as models which are made and calibrated to mimic nature to the greatest degree. Any stellar population model, such as STARLIGHT (BC03), is based on a stellar library. Usually, the stellar library does not sample a sufficiently wide range in metallicity, making stellar metallicity notoriously more difficult to access than other properties. Also, to get the metallicity correct, one must have correct ages, as they affect one another in these integrated spectral fits. Since our derived stellar ages have large uncertainties, the stellar metallicities are necessarily also poorly constrained. So, stellar metallicities determined here from stellar population synthesis (Table 5) carry large uncertainties, and are not reliable as specific values for comparisons and scientific studies; the gas-phase metallicities (Table 3) from the emission-line flux ratios are much more reliable.

6.1.2. Effect of Blue Light Loss on Conclusions

We use the blue-side spectra for studying stellar populations by full-spectrum fitting, so the accuracy of the relative flux calibration becomes an important factor for the reliability of the stellar population results. If the slit is not positioned along the atmospheric dispersion, the light loss at blue-end wavelengths would be greater than that at red-end wavelengths. As shown in Table 2 in Section 3.2, if a star was being centered at 6000 Å and observed with the same slit positioning schemes and observing configurations as those

in our program, it will be off center by $0.61''$ at 3600 \AA and $0.05''$ in the opposite direction at 6500 \AA for AGC 191770, by $0.8''$ at 3600 \AA and $0.06''$ in the opposite direction at 6500 \AA for AGC 228010, and by $0.8''$ at 3600 \AA and $0.06''$ in the opposite direction at 6500 \AA for AGC 253926. The light loss at 3600 \AA is (respectively) 4.8%, 15.2%, and 0.6% greater than that at 6500 \AA for AGC 191770, AGC 228010, and AGC 253926.

Obviously, the relative blue-light loss of AGC 228010 is the largest among the three galaxies. However, such an amount of light loss is calculated under the assumption that our targets were stars. Actually, as seen in Figure 2, they are galaxies with extended areas larger than the slit width. So, the lost blue light is partly gained back from the neighboring pixels, and the effect on relative flux calibration of blue-end spectra is not that significant, although it still exists. The probable light loss at blue-end wavelengths ($\sim 3600 \text{ \AA}$) would cause an underestimate of late A-type stars. Even with some blue-light loss, we could still obtain the same qualitative conclusion that these three LSBGs have a potential dearth of stars with ages $< 1 \text{ Gyr}$ because late A-type stars typically have ages older than $\sim 1 \text{ Gyr}$.

6.1.3. *Limitations Caused by Very Small Sample*

Limited by the reliability of a spectral continuum, the number of spectra that we can use for a possibly reliable conclusion from full-spectrum fitting is only three. Undoubtedly, this is from a representative sample of the whole edge-on LSBG sample, and not even representative of our final 12 observing targets. Thus, conclusions from the three galaxies may not apply more generally to LSBGs. To get more universal conclusions on stellar populations of LSBGs, we will seek sufficient observing time in the future, obtaining stellar continuum spectra of good quality for a larger and more representative sample of edge-on LSBGs.

Table 4. Estimated Stellar Mass and Gas Mass Fraction of Edge-on LSBGs

AGC No.	$\log(M_\star/M_\odot)_{B-V}$	$\log(M_\star/M_\odot)_{\text{SDSS}}$	$f_{g,B-V}$	$f_{g,\text{SDSS}}$
191770	7.89	8.39	0.96	0.87
228010	7.95	8.37	0.98	0.94
253926	9.11	9.96	0.95	0.73
12249	9.21		0.82	
321228	8.82		0.79	
332804	9.20	9.88	0.90	0.64
332806	8.70	9.46	0.95	0.76
100811	9.09	9.79	0.87	0.57
123165	8.64		0.74	
101807	9.11	9.88	0.93	0.70
1181	9.00	9.68	0.92	0.71
748835	9.09		0.91	

Table 5. Stellar Population Synthesis Results for Three Edge-on LSBGs

Parameter	Galaxy Name					
	AGC 191770		AGC 228010		AGC 253926	
	CAL	CCM	CAL	CCM	CAL	CCM
$\log(\text{age}_L)$	8.8	8.7	9.0	9.0	8.9	8.7
$\log(\text{age}_M)$	9.1	9.1	9.0	9.0	9.3	9.0
Z_L^{a}	0.030	0.030	0.050	0.050	0.037	0.040
Z_M	0.045	0.047	0.050	0.050	0.040	0.049
A_V (mag)	0.18	0.24	0.00	0.00	0.91	0.99
$\text{LF}_{\text{YSP}}^{\text{b}}$	0.0	0.0	0.0	0.0	9.4	11.2
LF_{OSP}	100.0	100.0	100.0	100.0	90.6	88.8
$\text{MF}_{\text{YSP}}^{\text{c}}$	0.0	0.0	0.0	0.0	0.04	0.1
MF_{OSP}	100.0	100.0	100.0	100.0	99.96	99.9

^a Z refers to the mass fraction of all “metals” of a star. Z_L and Z_M refer to metallicities of luminosity-weighted and mass-weighted stellar populations, respectively.

^bF refers to light fraction to the total light.

^cMF refers to mass fraction to the total stellar mass.

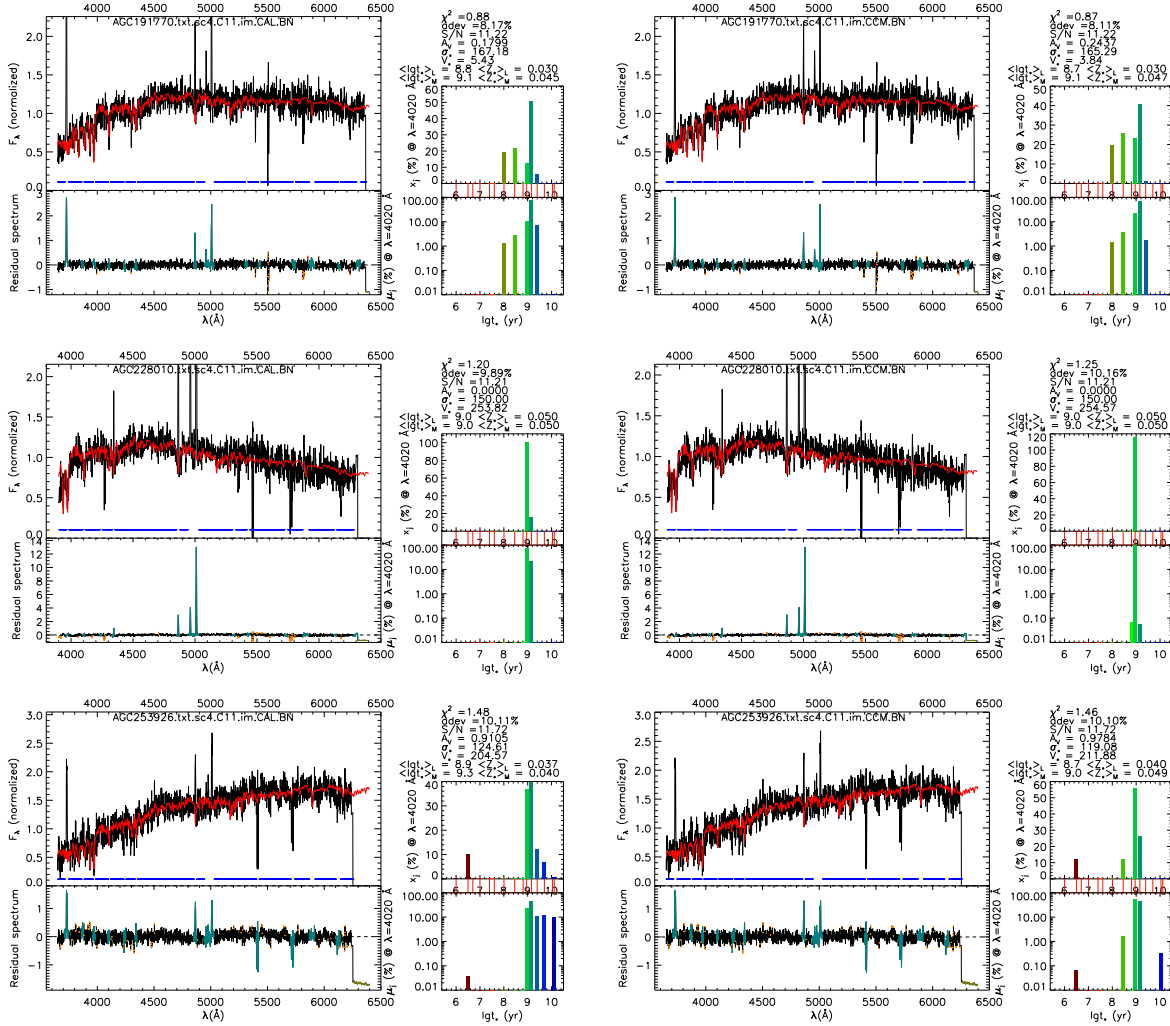


Fig. 7.— STARLIGHT stellar population synthesis results for three edge-on LSBGs. The left and right columns are respectively for the CAL and CCM reddening laws. In each panel, the top-left part shows the observed spectrum (black) and the STARLIGHT fit (red). The blue line is the error spectrum, with gaps marking bad pixels. However, we have not extracted the error spectrum from our data, so the blue line here is simply a horizontal line of value 0. The bottom-left part shows the residual spectrum, with cyan corresponding to masked windows (e.g., emission lines) and yellow marking clipped pixels (e.g., bad sky subtraction). The plots at right show age distributions of the resulting stellar populations expressed as a light fraction (top) and a mass fraction (bottom). The bar-code panel (between the top-right and bottom-right parts) indicates the ages of all stellar populations included during the fit.

6.2. Stellar Mass

In Figure 6, the gas mass fractions computed from two different sets of stellar masses for our sample have obvious discrepancies. The gas mass fractions from the “*B*-based” stellar masses are apparently higher than those from the “*z*-based” stellar masses.

Which set of stellar mass is more appropriate for LSBGs? Here, we prefer the “*z*-based” stellar masses because of the following reasons: (1) The luminosity at relatively longer wavelengths (the red or near-infrared bands) is more ideal for tracing the stellar mass because it is less affected by extinction and other factors that affect shorter-wavelength bands. (2) LSBGs have few blue, massive stars formed in the past 1 Gyr; the stellar mass is predominantly in low mass stars which radiate most of their light at red and near-infrared wavelengths. We checked the *WISE* satellite 3.4 μm and 4.6 μm images of our LSBGs and found that all of them are detected in both bands, especially in the bulge regions. Thus, the stellar masses of LSBGs would be underestimated from their *B*-band luminosity. (3) The “*z*-based” stellar masses of our LSBG sample are $M_\star \approx 10^{8.0} - 10^{10.0} M_\odot$, which agrees with the conclusion of other studies that LSBGs are mostly comparable in mass with prominent spirals that define the Hubble sequence (e.g., McGaugh 1994).

6.3. Chemical Evolution of LSBGs

In the closed-box model of the chemical evolution of galaxies, the initially metal-free gas is permanently locked into stars with neither inflow nor outflow and only evolves “in isolation” with time. Other assumptions include an invariant stellar initial mass function and instantaneous recycling. The relation between the metallicity (Z) and the gas mass fraction (f_g) for a system that evolves in isolation is

$$Z = y \ln(1/f_g), \quad (3)$$

where y is the “yield,” the ratio of the mass of newly formed metals to the mass of gas permanently locked in stars. Here, Z is best expressed as an elemental abundance in logarithmic form. For oxygen, following Lee et al. (2003), this equation can be rewritten as

$$\log Z_{\text{O}} = \log y_{\text{O}} + \log \ln(1/f_g), \quad (4)$$

$$12 + \log (\text{O}/\text{H}) = 12 + \log (0.196y_{\text{O}}) + \log \log(1/f_g). \quad (5)$$

In a plot of oxygen abundance, $12 + \log(\text{O}/\text{H})$, against inverse gas mass fraction, conveyed by $\log \log(1/f_g)$, the closed-box model predicts a slope of unity. Deviations from this slope may be an indication for the inflow or outflow of gas. The oxygen yield, y_{O} , can be derived from the intercept of the plot.

Following Lee et al. (2003), for the field dIrrs, there is an excellent correlation represented by a line with a slope of unity (green solid line in Figure 6) which is consistent with the closed-box model of the chemical evolution of galaxies. The standard deviation of the fit is 0.126 dex in $\log(\text{O}/\text{H})$. From the intercept of the line, the effective oxygen yield by mass (y_{O}) for the field dIrrs from Lee et al. (2003) is 2.22×10^{-3} . Obviously, the LSBG data (purple open triangles) from de Naray (2004) are generally consistent with the field dIrr data (green open squares) and can also be fitted by the closed-box model fit (green solid line) of Lee et al. (2003), albeit with more scatter.

We cannot tell for sure whether our LSBG sample can be explained with the closed-box model by fitting; our sample is too small and also too narrow in the coverage of both gas mass fraction and gas-phase metallicity to show a true relation, even if some essential relations do indeed exist. However, to compare with the field dIrrs from Lee et al. (2003)

and the LSBGs from de Naray (2004), we still forced our LSBG data (all filled circles with “ z -based” stellar mass) to be fitted by a line with a slope of unity (red solid line). The standard deviation of this fit is 0.27 dex in $\log(\text{O}/\text{H})$. From this artificial fitting, the effective oxygen yield by mass for our LSBG sample is 6.23×10^{-3} under the assumption of a closed-box model. The value of true yield is often considered to be the solar oxygen abundance by mass. For the Sun, the oxygen abundance is $12 + \log(\text{O}/\text{H}) = 8.87$ dex (Grevesse et al. 1996; Lee et al. 2003), which is 9.00×10^{-3} by mass. Apparently, the effective oxygen yield for our LSBG sample is larger than that for the dIrr sample, and is 69% of the value for the true oxygen yield. The difference between the effective and true yields roughly represents the fraction of metal lost (up to 30%) up to now (Garnett 2002).

Such a value of metal loss can be reasonable since it is often argued that LSBGs have shallow potential wells, making it easier for mass loss to occur. However, given the substantial uncertainties in both metallicity and gas mass fraction for our LSBG sample, this mass-loss value of 30% is only a rough estimate, and we cannot completely rule out a closed-box scenario. Additionally, judging from the offset between the two closed-box lines in Figure 6, we find evidence that our LSBGs retain up to ~ 3 times as much of their metals compared with dwarf irregulars (green squares), consistent with metal retention being related to galaxy mass. In any case, although the closed-box scenario cannot be completely ruled out for our LSBG sample, there is still substantial room for considering other, more complicated chemical evolution models with outflow or even infall (e.g., Edmunds 1990; Chang et al. 2010) for our LSBG sample.

6.4. Are LSBGs a Fundamentally Different Type?

In the z -based stellar masses (Table 4), our LSBG sample is estimated to be $10^{8.3} - 10^{10.0} M_{\odot}$, showing no fundamental differences from prominent spiral galaxies. Furthermore,

comparing with previously published luminosity-metallicity plots for LSBGs and other galaxy types (Figure 4), our LSBG sample agrees well with the LSBG sample of de Naray (2004) and also generally the sample of normal galaxies. In the mass-metallicity plot (Figure 5), our LSBG sample is also consistent with the LSBG sample of de Naray (2004) and with the relatively low abundance for their stellar mass, which is appropriate for normal galaxies. Therefore, from the behavior in the $L-Z$ and $M-Z$ plots, our LSBG sample does not seem to be fundamentally different from normal disk galaxies.

Regarding the plot of gas mass fraction versus oxygen abundance (Figure 6), we prefer the z -based stellar masses (black or red filled circles). Our LSBG sample is not likely to be explained by simple closed-box models, although the galaxies evolve in relative isolation. Systematically biased to larger gas mass fractions, our LSBG sample has higher oxygen abundances for smaller gas mass fractions, which is also shown by other samples. Such qualitative agreement in gas mass fraction versus metallicity distribution makes the LSBGs seem consistent with other galaxy types.

We therefore suggest that LSBGs are probably not fundamentally different from normal galaxies, but are just the continuous extension to the lower surface-brightness end of normal disk galaxies.

7. Conclusions

We have obtained long-slit spectra of 12 edge-on LSBGs selected from the EGIS- α .40 sample. Observations were made with the Kast spectrograph on the 3-m Shane telescope at Lick Observatory for 3 galaxies and with the Double Spectrograph on the 5-m Hale telescope at Palomar Observatory for 9 galaxies. We adopted a median-filter method to estimate the sky background of objects observed at Lick Observatory and a second-order

polynomial to fit the sky background of objects observed at Palomar Observatory, which can be comparable to or even exceed the galaxy surface brightnesses.

The stellar populations of three of the LSBGs were studied with the program STARLIGHT, as their spectral quality is sufficiently high. We find that our LSBGs are dominated by stellar populations with ages > 1 Gyr and have a potential dearth of stars with ages < 1 Gyr. This indicates that LSBGs probably have a very low level of star-formation activity over the past 1 Gyr, which may be the most likely explanation for their low surface brightness.

We have measured oxygen abundances ($12 + \log(\text{O}/\text{H})$) using both the R_{23} and $[\text{N II}]/\text{H}\alpha$ diagnostics after performing reddening corrections for the observed fluxes of emission lines. The R_{23} -based metallicities are 8.00–8.62, with a mean of 8.30 dex and a median of 8.26 dex. The $[\text{N II}]/\text{H}\alpha$ -based metallicities are 7.67–8.54, with a mean of 8.20 dex and a median of 8.26 dex. The two sets of oxygen abundances are consistent with each other. Comparing with the luminosity-metallicity relation established in previous work on LSBGs, normal spirals, and other galaxy types, our LSBGs tend to be consistent with normal galaxies.

We derive two sets of stellar masses for our LSBG sample. One set is the z -based stellar masses which are $10^{8.0}$ – $10^{10.0} M_{\odot}$, and the other set is the B -based stellar masses which are $10^{7.5}$ – $10^{9.5} M_{\odot}$, 0.5 order of magnitude lower. We argue that the z -based stellar masses are better for our LSBG sample because such galaxies primarily consist of low mass stars which radiate their light mostly at red and infrared wavelengths. Stellar masses derived from the B band might be underestimated. According to the z -based stellar masses, our LSBGs are comparable to normal spiral galaxies in stellar mass, but they have considerably lower abundances.

In the plot of gas mass fraction versus oxygen abundance, we find that like other galaxy

types, our LSBGs with relatively high “ z -based” stellar masses have lower metallicities for higher gas mass fractions. Regarding the chemical evolution of our sample, the LSBG data appear to allow for up to 30% metal loss, but we cannot completely rule out the closed-box model. Additionally, we find evidence that our galaxies retain up to about 3 times as much of their metals compared with dwarfs, consistent with metal retention being related to galaxy mass.

Combining the above conclusions, our LSBG sample is generally consistent with the luminosity-metallicity, mass-metallicity, and gas mass fraction-metallicity plots of normal spiral galaxies and other galaxy types (e.g., dIrrs, starbursts). Thus, we speculate that LSBGs are probably not fundamentally different from normal galaxies, but rather are just the continuous extension in surface brightness to the low end.

We acknowledge the anonymous referee for whose detailed comments helped strengthen this paper. This research uses data obtained through the Telescope Access Program (TAP), which has been funded by the National Astronomical Observatories of China, the Chinese Academy of Sciences (the Strategic Priority Research Program “The Emergence of Cosmological Structures” Grant No. XDB09000000), and the Special Fund for Astronomy from the Ministry of Finance. Three observational nights (20–22 Sep. 2015) with the Double Spectrograph on the 5-m Hale telescope were distributed to us for scientific studies of LSBGs via the TAP. Observations obtained with the Hale Telescope at Palomar Observatory were obtained as part of an agreement between the National Astronomical Observatories, Chinese Academy of Sciences, and the California Institute of Technology. Additionally, we are grateful to the staffs of Lick and Palomar Observatories for their assistance with the observations. Research at Lick Observatory is partially supported by a generous gift from Google. W. Du thanks Cheng Cheng, Zhimin Zhou and Fan Yang in NAOC for discussions concerning data reduction, and thanks Ruixiang Chang in SHAO for

helpful suggestions during revision.

This work is supported by the National Natural Science Foundation of China (Grant Nos. 11403037, 11225316, and 11173030), the Strategic Priority Research Program “The Emergence of Cosmological Structures” of the Chinese Academy of Sciences (Grant No. XDB09000000), and the Key Laboratory of Optical Astronomy, NAOC. A.V.F. has received generous financial assistance from the Christopher R. Redlich Fund, the TABASGO Foundation, and NSF grant AST-1211916.

Facilities: Palomar Hale (DBSP), Lick Shane (Kast)

REFERENCES

- Abazajian K. N., Adelman-McCarthy J. K., Agueros M. A. et al. 2009, *ApJS*, 182, 543
- Bell E. F., McIntosh D. H., Katz N., Weinberg M. D. 2003, *ApJS*, 149, 289
- Bizyaev D. V., Kautsch S. J., Mosenkov A. V. et al. 2014, *ApJ*, 787, 24
- Bothun G. D., Impey C. D., Malin D. F., Mould J. R. 1987, *AJ*, 94, 23
- Bothun G. D. et al. 1997, *PASP*, 109, 745
- Brodie J. P., Huchra J. P. 1991, *ApJ*, 379, 157
- Bruzual G., Charlot S. 2003, *MNRAS*, 344, 1000
- Burkholder V., Impey C., Sprayberry D. 2001, *AJ*, 122, 2318
- Calzetti D., Armus L., Bohlin R. C. et al. 2000, *ApJ*, 533, 682
- Cardelli J. A., Clayton G. C., Mathis J. S. 1989, *ApJ*, 345, 245
- Ceccarelli L., Herrera-Camus R., Lambas D. G., Galaz G., Padilla N. D. 2012, *MNRAS*, 426, 6
- Chang R. X., Hou J. L., Shen S. Y., Shu C. G. 2010, *ApJ*, 722, 380
- Cid Fernandes R., Mateus A., Sodre L., Stasinska G., Gomes J. M. 2005, *MNRAS*, 358, 363
- Cole S., Norberg P., Baugh C. M. et al. 2001, *MNRAS*, 326, 255
- de Grijs R. 1998, *MNRAS*, 299, 595
- de Blok W. J. G., McGaugh S. S. 1998, *ApJ*, 508, 132
- de Blok W. J. G., van der Hulst J. M. 1998, *A&A*, 336, 49

- de Naray R., McGaugh S., de Blok W. 2004, MNRAS, 355, 887
- Das M. et al. 2009, ApJ, 693, 1300
- Denicolo G., Terlevich R., Terlevich E., 2002, MNRAS, 330, 69
- Disney M. J. 1976, Nature, 263, 573
- Du W., Wu H., Lam M.-I. et al. 2015, AJ, 149, 199
- Edmunds M. G. 1990, MNRAS, 246, 678
- Edmunds M. G. 1999, in Davies J. I., Impey C., Phillips S., ed., ASP Conf. Ser. Vol.170,
The Low Surface Brightness Universe. Astron. Soc. Pac., San Francisco, p. 383
- Faber S. M. 1973, ApJ, 179, 731
- Filippenko A. V. 1982, PASP, 94, 715
- Galaz G. et al. 2011, ApJ, 728, 74
- Garnett D. R., Shield G. A. 1987, ApJ, 317, 82
- Garnett R. D. 2002, ApJ, 581, 1019
- Grevesse N., Noels A., Sauval A. J. 1996, in ASP Conf. Ser. 99, Cosmic Abundances:
Proceedings of the 6th Annual October Astrophysics Conference, ed. S. S. Holt & G.
Sonneborn (San Francisco: ASP), 117
- Haberzettel L. et al. 2007, A&A, 471, 787
- Haynes M. P., Giovanelli R., Martin A. M. et al. 2011, AJ, 142, 170
- Impey C. & Bothun G. 1997, AR&AA, 35, 267
- Impey C., Burkholder V., Sprayberry D. 2001, AJ, 122, 2341

- Kauffmann G., Heckman T. M., White S. D. M. et al. 2003, MNRAS, 314, 33
- Kelson D. D. 2003, PASP, 155, 688
- Kewley L. J. & Dopita M. A. 2002, ApJS, 142, 35
- Kochanek C. S., Pahre M. A., Falco E. E. et al. 2001, ApJ, 560, 566
- Lam M. I., Wu H., Yang M. et al. 2015, MNRAS, 446, 4291
- Lamareille F., Mouhcine M., Contini T., Lewis I., Maddox S. 2004, MNRAS, 350, 396
- Lee H., McCall M. L., Kingsburgh R. L., Ross R., Stevenson C. C. 2003, AJ, 125, 146
- Lequeux J., Peimbert M., Rayo J. F., Serrano A., Torres-Peimbert S. 1979, A&A, 80, 155
- Liang Y. C. et al. 2010, MNRAS, 409, 213
- Matthews L. D. & Gallagher J. S. AJ, 114, 1899
- Matthews L. D. & Wood K. 2001, ApJ, 548, 150
- McGaugh S. S., 1991, ApJ, 380, 140
- McGaugh S. S. 1994, ApJ, 426, 135
- McGaugh S. S. 1996, MNRAS, 280, 337
- McGaugh S. S., de Blok W. J. G. 1997, ApJ, 481, 689
- McGaugh S. S. & Bothun G. D. 1994, AJ, 107, 530
- Melbourne J., Salzer J. J. 2002, AJ, 123, 2302
- Miller J. S. & Stone R. P. S. 1993, Lick Obs. Tech. Rep. 66 Santa Cruz: Lick Obs.
- Minchin R. F. et al. 2004, MNRAS, 355, 1303

- Morelli L., Corsini E. M., Pizzella A. et al., 2012, MNRAS, 423, 962
- Oke J. B. & Gunn J. E. 1982, PASP, 94, 586
- O’Neil K. et al. 2000, AJ, 119, 136
- Osterbrock D. E. 1989, *Astrophysics of Gaseous Nebulae and Active Galactic Nuclei* (Mill Valley, CA: University Science Books)
- Pagel B. E. J. et al. 1979, MNRAS, 189, 95
- Pettini M. & Pagel B. E. J., 2004, MNRAS, 348, L95
- Schombert J. M., Bothun G. D., Impey C. D., Mundy L. G. 1990, AJ, 100, 1523
- Schombert J., McGaugh S. S., Eder J. A. 2001, AJ, 121, 2420
- Schombert J. et al. 1992, AJ, 103, 1107
- Schombert J. et al. 2013, AJ, 146, 41
- Skillman E. D., Kennicutt R. C., Hodge P. W. 1989, ApJ, 347, 875
- Smith J. A., Tucker D. L., Kent S., Richmond M. W. et al. 2002, AJ, 123, 2121
- Trachternach C., Bomans D. J., Haberzettl L., Dettmar R. J. 2006, A&A, 458, 341
- Tremonti C. A., Heckman T. M., Kauffmann G. et al. 2004, ApJ, 613, 898
- van Dokkum P. G. 2001, PASP, 113, 1420
- van der Hulst J. M. et al. 1993, AJ, 106, 548
- van der Kruit P. C. 1981, A&A, 99, 298
- van der Kruit P. C. 1988, A&A, 192, 117

van der Kruit P. C., Kregel M., Freeman C. K. 2001, *A&A*, 379, 374

Wen X. Q., Wu H., Zhu Y. N. et al. 2013, *MNRAS*, 433, 2946

Wu H., Cao C., Hao C. N. et al. 2005, *ApJ*, 632, 79

Zaritsky D., Kennicutt Jr. R. C., Huchra J. P. 1994, *ApJ*, 420, 87

Zhu Y. N., Wu H., Li H. N., Cao C. 2010, *RAA*, 10, 329